CMI growth rates for Saturnian Kilometric Radiation

R. L. Mutel, J. Menietti, Donald A. Gurnett, William S. Kurth, Patricia Schippers, C. Lynch, Laurent Lamy, Christopher S. Arridge, Baptiste Cecconi

CMI growth rates for Saturnian kilometric radiation

R. L. Mutel,[1] J. D. Menietti,[1] D. A. Gurnett,[1] W. Kurth,[1] P. Schippers,[1] C. Lynch,[1] L. Lamy,[2] C. Arridge,[2] and B. Cecconi[3]

Received 2 August 2010; revised 3 September 2010; accepted 7 September 2010; published 15 October 2010.

[1] We calculate growth rates for extraordinary mode Saturnian kilometric radiation generated by the electron cyclotron maser instability using a ring-type (DGH) electron phase distribution model fitted to measured electron energy distributions in Saturn's auroral acceleration region. The observed distributions are unstable in spatially isolated regions of transverse linear size of order 10^3 km. Each unstable region has a growth rate consistent with amplification of background radiation to the peak observed intensity, approximately 14 electric field e-foldings. The observed propagation direction and frequency decrement below the electron cyclotron frequency are also consistent with the CMI growth model.
Citation: Mutel, R. L., J. D. Menietti, D. A. Gurnett, W. Kurth, P. Schippers, C. Lynch, L. Lamy, C. Arridge, and B. Cecconi (2010), CMI growth rates for Saturnian kilometric radiation, *Geophys. Res. Lett.*, *37*, L19105, doi:10.1029/2010GL044940.

1. Introduction

[2] Intense low-frequency radio emission is routinely detected from all planets with global magnetospheres [*Zarka*, 2002]. The emission, denoted variously as auroral kilometric radiation (AKR, Earth), decametric radiation (DAM, Jupiter), and Saturnian kilometric radiation (SKR, Saturn), is highly polarized, narrowly beamed [*Mutel et al.*, 2007; *Imai et al.*, 2008], and originates above each planet's auroral regions [*Gurnett and Green*, 1978; *Huff et al.*, 1988; *Mutel et al.*, 2004]. The radiation is generated by conversion of free energy from unstable electron phase distributions via the cyclotron maser instability (CMI) [*Wu and Lee*, 1979; *Treumann*, 2006]. The instability results from mildly relativistic, downward-directed electron beams accelerated by parallel electric fields. As the electron beams encounter increasing magnetic field at lower altitude, the parallel energy is converted to perpendicular energy, resulting in a unstable positive perpendicular velocity gradient. This drives strong wave growth near the local electron cyclotron frequency.

[3] The CMI maser mechanism and its corresponding AKR emission have been well-studied at Earth, both by remote sensing of the radiation and by in situ measurements of electron energies and phase distributions at the source. Early papers, based on measured phase distribution functions with inadequate energy and pitch-angle resolution, assumed that the CMI instability was driven by the positive gradient along the borders of a loss-cone oriented in the upward parallel direction [e.g., *Wu et al.*, 1982; *Omidi and Gurnett*, 1982]. However, the growth rates derived from loss-cone models required implausibly large convective growth lengths [*Omidi et al.*, 1984]. More recent observations of the electron velocity distribution function found that single and multiple shell distributions with energies between 1–10 keV were present in the auroral cavities [*Delory et al.*, 1998; *Su et al.*, 2007], and that these distributions provided a much more robust CMI growth rate [*Louarn and Le Quéau*, 1996; *Pritchett et al.*, 2002; *Mutel et al.*, 2007].

[4] Although the case for CMI-generated terrestrial AKR is now well-established, until recently the same analysis had not been possible for other planetary magnetospheres, since spacecraft probes had never traversed extraterrestrial auroral acceleration regions. However, in Fall 2008 the Cassini spacecraft crossed the Saturnian auroral region for the first time. During one epoch (17 Oct 2008) the observed radio spectrum dipped slightly below the local electron gyrofrequency, a clear indication that the spacecraft was at or very close to the SKR source region. *Lamy et al.* [2010] have recently summarized the properties of SKR observed during this event. In this companion paper, we show that CMI growth rates derived from the observed electron phase distributions measured within the SKR source region are consistent with observed SKR properties, including spectral intensity, propagation direction, and frequency decrement relative to the local electron cyclotron frequency.

2. CMI Growth Rate

[5] Nearly all observed terrestrial AKR and Kronian SKR radiation produced by the CMI mechanism is dominated by the extraordinary (X) mode [*Gurnett and Green*, 1978; *Treumann*, 2006; *Lamy et al.*, 2008], although much weaker O-mode radiation is sometimes observed [*Mellott et al.*, 1984; *Lamy et al.*, 2008]. In this paper, we are concerned only with growth rates for the dominant X-mode process. For this mode, the CMI growth rate can be written [*Mutel et al.*, 2007],

$$\frac{\omega_i}{\Omega} = \frac{\pi^2}{4}\frac{n_h}{n_e}\beta^2 v_r^2 \int_0^{\pi} d\varphi \, \sin^2\varphi \left[\frac{\partial f}{\partial v_\perp} + \frac{k_\parallel v_\perp}{\Omega}\frac{\partial f}{\partial v_\parallel}\right]_{|\vec{v}|=v_r} \quad (1)$$

where ω_i is the imaginary part of the angular frequency, Ω is the electron cyclotron frequency, n_h is the number density of 'hot' electrons, i.e., those contributing to the instability, n_e is the total electron number density, β is the ratio of electron plasma to gyrofrequencies, f is the normalized phase distribution function, ($v_\perp$, $v_\parallel$) are the components of the velocity perpendicular and parallel to the magnetic field, and $k_\parallel$ is the parallel component of the wave normal vector.

[1]Department of Physics and Astronomy, University of Iowa, Iowa City, Iowa, USA.
[2]Space and Atmospheric Physics, Imperial College London, London, UK.
[3]Observatoire de Paris, Meudon, France.

0094-8276/10/2010GL044940

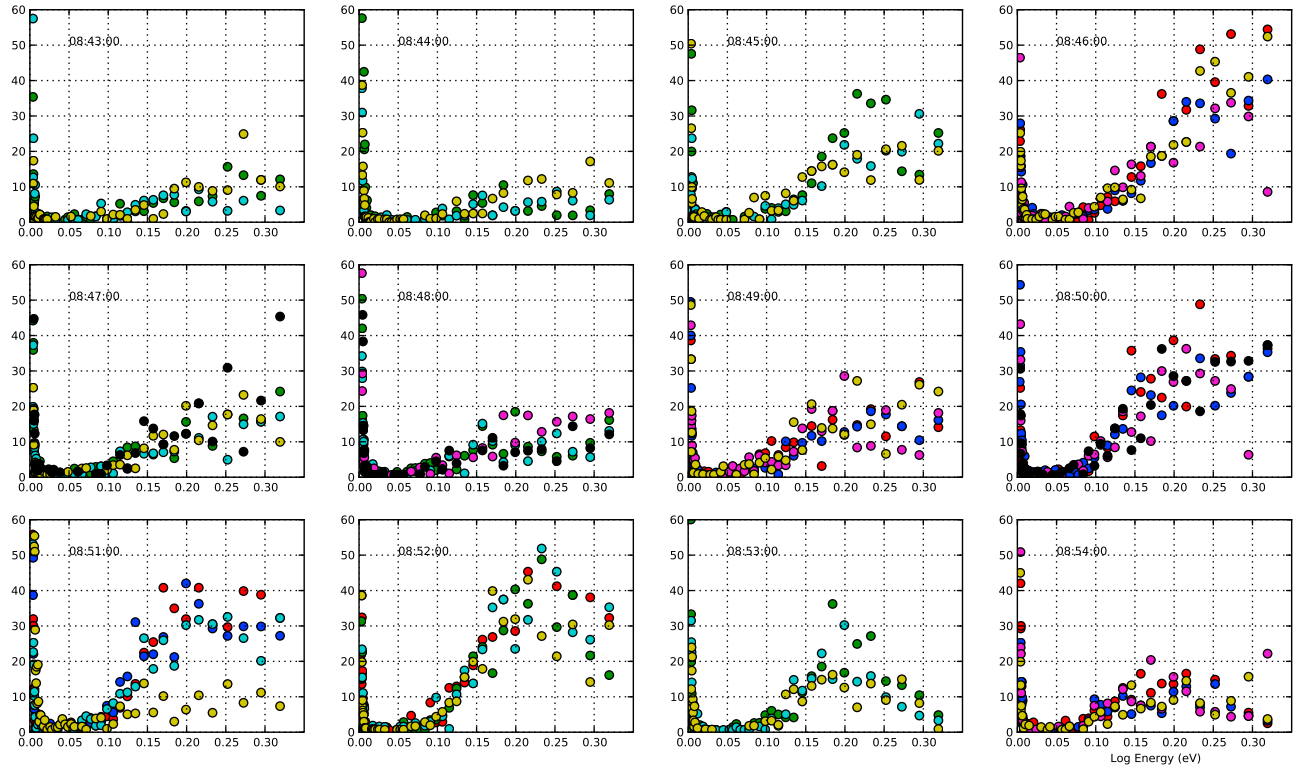

Figure 1. Twelve 2-second CAPS electron velocity distribution functions at fixed pitch angles spaced at one minute intervals on 17 Oct 2008 from 08:43–08:54 UT. The densities have been de-trended by dividing by a background kappa distribution as described in the text. Colors indicate samples at pitch angle: 65° (red), 75° (green), 85° (blue), 95° (cyan), 105° (maroon), 115° (yellow), and 125° (black). Note the growth and decay of the unstable distributions near 08:46 and 08:53.

The integration path is along the resonance ellipse, which for $v \ll c$ is a circle given by the constraint

$$v_r^2 = v_\perp^2 + \left(v_\parallel - v_c\right)^2$$

with radius

$$v_r = \left(v_c^2 - 2\delta\omega\right)^{\frac{1}{2}}$$

and center $v_c = k_\parallel c/\Omega$ offset along the $v_\parallel$ axis, and the normalized frequency is $\delta\omega = (\omega - \Omega)/\Omega$. We have normalized velocities to the speed of light and the phase distribution function f so that its integral over velocity space is unity.

2.1. Measured Electron Phase Space Density

[6] The CAPS-ELS instrument [*Linder et al.*, 1998; *Young et al.*, 2004] measures the 2-dimensional electron phase distribution function in the energy range from 0.58 eV to 26 keV in 63 logarithmically spaced energy channels. The electron pitch angle distribution is sampled using eight anodes positioned on a rotating platform. This scheme provides 160° coverage in elevation and 208° coverage in azimuth, although it requires 180 sec to sample the full angular range. This is problematic for CMI growth rate calculations since an unstable electron population may have a lifetime shorter than a few minutes.

[7] Fortunately the CAPS instrument also allows fast (2-sec) sampling of the current subset of pitch angles being sampled. Although each 2-sec record is an incomplete representation of the full 2-dimension distribution, in most records there is sufficient coverage of the perpendicular component (near 90° pitch angle) to allow a reasonable estimate of the perpendicular gradient. By visual inspection of all 2-sec samples in the interval 07:00–9:00 UT on 17 Oct 2008 ($4.45 < R/R_s < 5.08$, $-50° < \lambda_m < -66.6°$, 23:49 < *MLT* < 01:10), we found many intervals in which the distribution exhibited an unstable ($df/dv_\perp > 0$) feature near 10 keV ($v/c \sim 0.2$). These intervals typically last 10–20 sec, followed by somewhat longer (3–5 min) intervals with much weaker or even undetectable unstable regions.

[8] This variability is illustrated in Figure 1, which shows a series of 2-sec distributions over twelve minutes separated by one-minute intervals. Each subplot has been de-trended by dividing by a kappa distribution [e.g., *Saito et al.*, 2000] representing the mean background level which we assume to be the same in all spectra. The ordinate scale is the (dimensionless) ratio of observed phase space density to the fitted background level. The pitch angle sampling, indicated by color-coded dots, is somewhat different for each record, but the overall trend is clear. For this twelve minute interval the largest unstable populations occur near 08:46 and 08:53 UT.

2.2. Analytic Model of Phase Space Density

[9] Figure 2a shows a single 2-sec CAPS distribution at 08:53:02 UT plotted in polar coordinates. The phase space density is shown using a color palette along seven pitch angles between 55° and 165°. Figure 2b shows the individual radial profiles for four pitch angles closest to the perpendicular direction, along with a best-fit model distri-

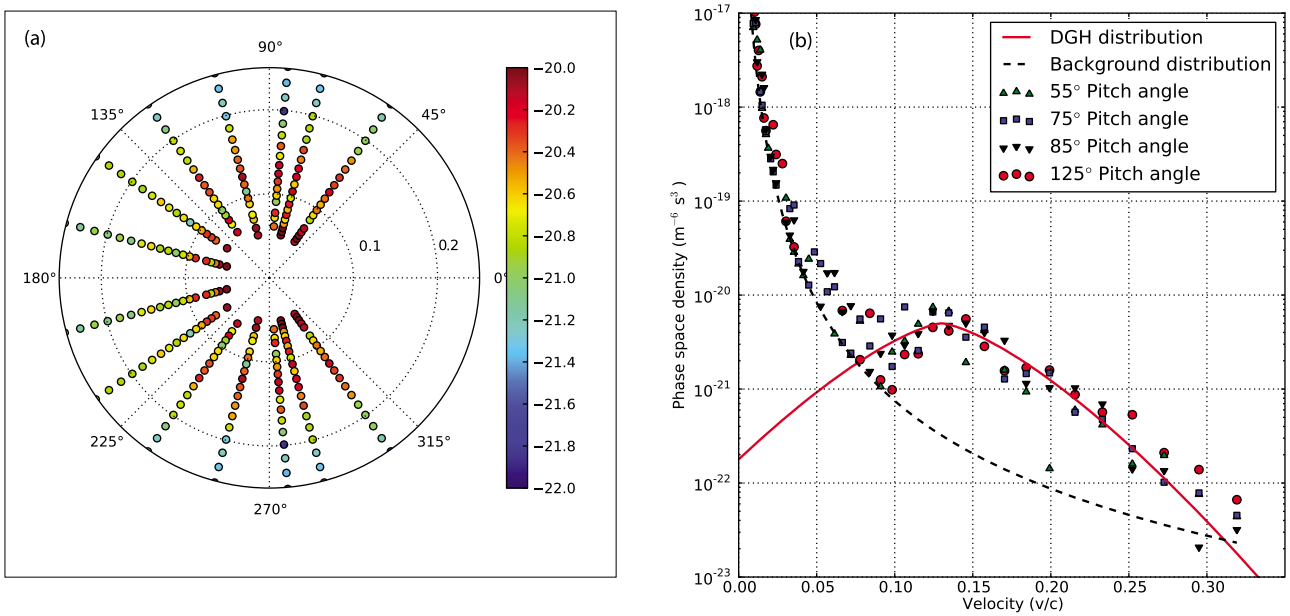

Figure 2. (a) CAPS electron velocity distribution function measured 18 Oct 2008 at 08:53:32 UT with 2-sec sampling. Sampled points with $|v| < 0.05c$ are suppressed. Number density is in logarithmic units of m^6 s^{-3}. Position angles are measured with respect to the magnetic field, so that 0° is toward Saturn (southern hemisphere). (b) One dimensional profiles of CAPS velocity distributions along 55° (triangles), 75° (squares), 85° (inverted triangles), and 125° (circles). The dashed black line is the kappa-distribution fitted background level, while the solid red line is a best-fit DGH distribution used to calculate the CMI growth rate.

bution used for growth rate calculations. The model consists of a kappa distribution fitted to the quiescent background plus a Dory-Guest-Harris (hereafter DGH) [*Dory et al.*, 1965] distribution for the unstable feature near 10 keV. The ambient plasma was assumed to have a mean density $n_e = 410^{-4}$ cm^{-3} ($\omega_{pe}/\Omega_{ce} = 0.06$) and a ratio of hot to total cold density $n_h/n_e = 0.2$, based on observed mean values during SKR source encounter [*Lamy et al.*, 2010]. We have used these parameters and the best-fit DGH model distribution to determine CMI growth rates.

[10] The resulting growth rate for X-mode radiation is shown in Figure 3a as a function of propagation angle and Figure 3b as a function of normalized frequency. The growth rate is strongly peaked near perpendicular propagation (90°), but with a half-width that depends on the normalized frequency $\delta\omega$.

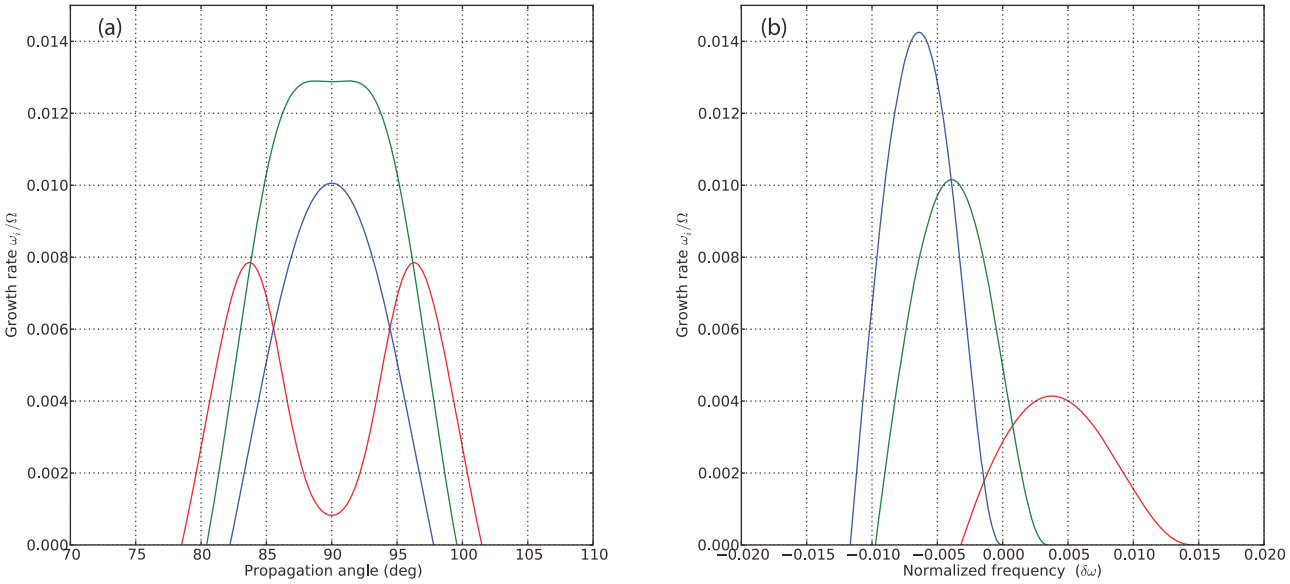

Figure 3. (a) Growth rate versus propagation angle with respect to the magnetic field for the DGH model fit to the measured CAPS phase distribution (Figure 2, dotted red line). The lines are for $\delta\omega/\delta\omega_{max} = 0.1$ (red line), 0.5 (blue line), and 0.9 (green line). (b) Growth rate versus normalized frequency $\delta\omega$ at propagation angles $\theta = 80°$ (red line), 85° (green line), and 90° (blue line).

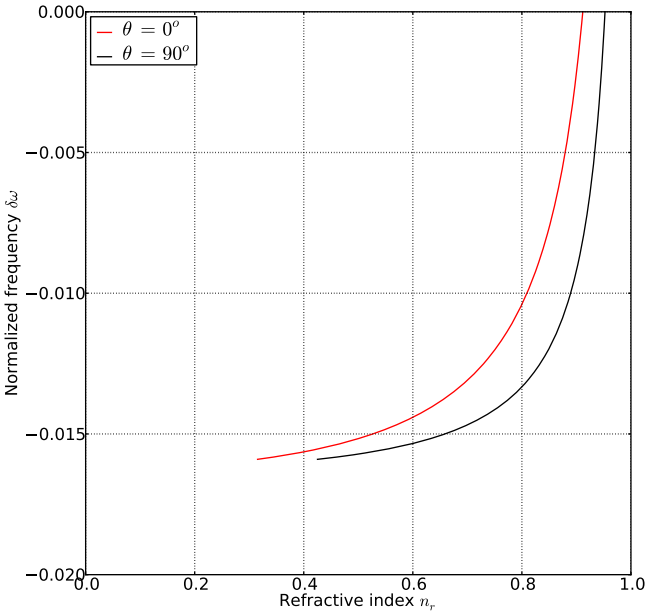

Figure 4. X-mode refractive index versus normalized frequency for propagation angles $\theta = 0°$ (red line) and $\theta = 90°$ (black line).

2.3. Comparison With Observed SKR Properties

[11] We now compare the observed properties of SKR (flux density, propagation direction, normalized frequency) during the 17 Oct 2008 Cassini encounter with the predicted properties of CMI-driven radiation based on the measured electron phase distribution as outlined above.

[12] The peak SKR specific intensity reported by *Lamy et al.* [2010] for the 17 October 2008 auroral crossing was 10^{-9} V^2 Hz^{-1}. This is equivalent to a flux density $S_{skr} \sim 6 \cdot 10^{-12}$ W m^{-2} Hz^{-1} using the conversion procedure for Cassini RPWS observations described by *Zarka et al.* [2004]. We assume that the CMI maser amplifies sky background photons. Estimates of the sky background flux density at low frequencies ($f < 100$ KHz) is problematic since such measurements are compromised by receiver noise or by quasi-thermal plasma noise near the spacecraft. However, we can estimate the background flux by noting that that sky brightness temperature between 100 KHz and 1 MHz is nearly constant, $T_B \sim 2 \cdot 10^7$ K [*Manning and Dulk*, 2001]. If we assume that this extends to lower frequencies, we find $S_{sky} \sim 6 \cdot 10^{-24}$ W m^{-2} Hz^{-1} at 10 KHz. Hence the observed intensity gain with respect to the background radiation field is

$$G_{obs} = \frac{S_{skr}}{S_{sky}} \sim 10^{12},$$

or equivalently, 14 e-foldings of the ambient E-field.

[13] In order to compare the intensity gain of the CMI maser with observed SKR intensities using the calculated growth rate, we first estimate the convective growth length, i.e., the spatial extent over which the conditions for CMI growth are nearly uniform. This depends on both spatial variations in the electron phase distribution and the strength and orientation of the magnetic field. Along a direction perpendicular to the magnetic field line, a dipole field varies as

$$\frac{\delta B_\theta}{B_\theta} \sim \frac{\delta B}{B} = \tan\theta\ \delta\theta$$

where θ is the magnetic latitude. The CMI maser will become incoherent if the local electron gyrofrequency along the path varies by more than the characteristic bandwidth. At Cassini's altitude during SKR source crossing ($R = 5R_s$), a normalized change $\delta\Omega/\Omega = \delta B/B = 0.01$ corresponds to a spatial scale $L_B = R \cdot \delta\theta \sim 5000$ km.

[14] As noted above, unstable electron distribution features have temporal timescales $\tau \sim 10$–20 sec in CAPS phase distributions. The relative speed of the Cassini spacecraft with respect to the magnetic field line is the vector sum of the orbital velocity in the Saturnian center of mass system and the co-rotation speed at the spacecraft distance, resulting in $V_r \sim 50$ km s^{-1} for period near 9:00 UT on 17 Oct 2008. This corresponds to a spatial scale for unstable regions $L_e = V_r u \sim 500$–1000 km. This is significantly smaller than the spatial scale of magnetic field variation, so we estimate the mean convective length scale as $L_c \sim 500$–1000 km.

[15] Given a growth rate ω_i, the CMI model intensity gain can be written

$$G_{cmi} = e^{2\omega_i t_c} = \exp\left[\frac{2\omega_i L_c}{V_g}\right],$$

where t_c is the convective growth timescale, and $V_g = d\omega/dk$ is the group velocity of the radiation. The group velocity can written [*Gurnett and Bhattacharjee*, 2005]

$$\mathbf{V_g} = c\left[\hat{\mathbf{k}}\frac{\partial\delta\omega}{\partial n} + \hat{\theta}\frac{1}{n}\frac{\partial\delta\omega}{\partial\theta}\right] \quad (2)$$

where $\hat{\mathbf{k}}$ and $\hat{\omega}$ are unit normal vectors in the k and θ directions respectively. Figure 4 shows $\delta\omega$ as a function of refractive index for both perpendicular and parallel propagation using a cold-plasma approximation with relativistic corrections using Lorentz factor $\gamma = 1.02$ (10 keV mean energy). We note that while the cold-plasma approximation may be strictly incorrect for plasmas with a significant warm component (as observed), dispersion calculations which properly account for the warm component [e.g., *Wong et al.*, 1982] find a similar results for the refractive index.

[16] Figure 4 shows that both terms in equation (2), while strongly dependent on $\delta\omega$, have comparable mean magnitudes, resulting in an average group velocity $V_g \sim 0.1c$. Using a mean CMI growth rate $\omega_i \sim 0.01 \cdot \Omega$, we find that the ambient E-field is amplified by 15 ± 5 e-foldings, or an intensity gain $log(G_{cmi}) = 13 \pm 4.4$. This encompasses the observed background amplification, although the high end is probably unrealistic, since it assumes a perfectly uniform unstable phase distribution along the entire 1,000 km convective growth path.

[17] The predicted propagation direction for maximum growth is perpendicular (Figure 3a), with significant CMI growth only over the relative narrow range $90° \pm 10°$. The observed propagation directions during SKR source crossings are larger, with a maximum deviation 20° from per-

pendicular [*Lamy et al.*, 2010]. These oblique rays may not be originating at the source, but may be refracted from sources located below the spacecraft.

[18] Finally, we address the frequency dependence of the growth rate. Figure 3b shows that the normalized frequency has a minimum lower bound $\delta\omega > -0.012$ at perpendicular propagation. This is largely consistent with observed frequency decrements, but with a few larger excursions, which occasionally dip below −0.02 [*Lamy et al.*, 2010, Figure 3]. This could result from episodic deviations of the electron phase distribution from the best-fit DGH model, but may also be a result of finite plasma temperature effects, which result in lower X-mode cutoff frequencies than given by cold plasma theory [*Winglee*, 1985].

3. Summary

[19] We have shown that the measured properties of SKR near $5R_s$ in Saturn's auroral regions result from conversion of free energy from an inverted population of electrons in a ring-type or shell distribution with radius near 10 keV via the cyclotron maser instability. There is no evidence for a loss-cone driven instability. The spatial extent of unstable regions is of order 1,000 km, separated by larger regions having little or no inverted populations.

References

Delory, G. T., R. E. Ergun, C. W. Carlson, L. Muschietti, C. C. Chaston, W. Peria, J. P. McFadden, and R. Strangeway (1998), FAST observations of electron distributions within AKR source regions, *Geophys. Res. Lett.*, *25*, 2069–2072, doi:10.1029/98GL00705.

Dory, R. A., G. E. Guest, and E. G. Harris (1965), Unstable electrostatic plasma waves propagating perpendicular to a magnetic field, *Phys. Rev. Lett.*, *14*, 131–133, doi:10.1103/PhysRevLett.14.131.

Gurnett, D. A., and A. Bhattacharjee (2005), *Introduction to Plasma Physics*, Cambridge Univ. Press, Cambridge, U. K.

Gurnett, D. A., and J. L. Green (1978), On the polarization and origin of auroral kilometric radiation, *J. Geophys. Res.*, *83*, 689–696, doi:10.1029/JA083iA02p00689.

Huff, R. L., W. Calvert, J. D. Craven, L. A. Frank, and D. A. Gurnett (1988), Mapping of auroral kilometric radiation sources to the aurora, *J. Geophys. Res.*, *93*, 11,445–11,454, doi:10.1029/JA093iA10p11445.

Imai, M., K. Imai, C. A. Higgins, and J. R. Thieman (2008), Angular beaming model of Jupiter's decametric radio emissions based on Cassini RPWS data analysis, *Geophys. Res. Lett.*, *35*, L17103, doi:10.1029/2008GL034987.

Lamy, L., P. Zarka, B. Cecconi, R. Prangé, W. S. Kurth, and D. A. Gurnett (2008), Saturn kilometric radiation: Average and statistical properties, *J. Geophys. Res.*, *113*, A07201, doi:10.1029/2007JA012900.

Lamy, L., et al. (2010), Properties of Saturn kilometric radiation measured within its source region, *Geophys. Res. Lett.*, *37*, L12104, doi:10.1029/2010GL043415.

Linder, D. R., A. J. Coates, R. D. Woodliffe, C. Alsop, A. D. Johnstone, M. Grande, A. Preece, B. Narheim, and D. T. Young (1998), The Cassini caps electron spectrometer, in *Measurement Techniques in Space Plasmas: Particles*, *Geophys. Monogr. Ser.*, vol. 102, edited by R. F. Pfaff, J. E. Borovsky, and D. T. Young, pp. 257–262, AGU, Washington, D. C.

Louarn, P., and D. Le Quéau (1996), Generation of the auroral kilometric radiation in plasma cavities—I. Experimental study, *Planet. Space Sci.*, *44*, 199–210, doi:10.1016/0032-0633(95)00121-2.

Manning, R., and G. A. Dulk (2001), The galactic background radiation from 0.2 to 13.8 mhz, *Astron. Astrophys.*, *372*, 663–666, doi:10.1051/0004-6361:20010516.

Mellott, M. M., W. Calvert, R. L. Huff, D. A. Gurnett, and S. D. Shawhan (1984), DE-1 observations of ordinary mode and extraordinary mode auroral kilometric radiation, *Geophys. Res. Lett.*, *11*, 1188–1191, doi:10.1029/GL011i012p01188.

Mutel, R., D. Gurnett, and I. Christopher (2004), Spatial and temporal properties of AKR burst emission derived from Cluster WBD VLBI studies, *Ann. Geophys.*, *22*, 2625–2632.

Mutel, R. L., W. M. Peterson, T. R. Jaeger, and J. D. Scudder (2007), Dependence of cyclotron maser instability growth rates on electron velocity distributions and perturbation by solitary waves, *J. Geophys. Res.*, *112*, A07211, doi:10.1029/2007JA012442.

Omidi, N., and D. A. Gurnett (1982), Growth rate calculations of auroral kilometric radiation using the relativistic resonance condition, *J. Geophys. Res.*, *87*, 2377–2383, doi:10.1029/JA087iA04p02377.

Omidi, N., C. S. Wu, and D. A. Gurnett (1984), Generation of auroral kilometric and Z Mode radiation by the cyclotron maser mechanism, *J. Geophys. Res.*, *89*, 883–895, doi:10.1029/JA089iA02p00883.

Pritchett, P. L., R. J. Strangeway, R. E. Ergun, and C. W. Carlson (2002), Generation and propagation of cyclotron maser emissions in the finite auroral kilometric radiation source cavity, *J. Geophys. Res.*, *107*(A12), 1437, doi:10.1029/2002JA009403.

Saito, S., F. R. E. Forme, S. C. Buchert, S. Nozawa, and R. Fujii (2000), Effects of a kappa distribution function of electrons on incoherent scatter spectra, *Ann. Geophys.*, *18*, 1216–1223.

Su, Y.-J., R. E. Ergun, S. T. Jones, R. J. Strangeway, C. C. Chaston, S. E. Parker, and J. L. Horwitz (2007), Generation of short-burst radiation through Alfvénic acceleration of auroral electrons, *J. Geophys. Res.*, *112*, A06209, doi:10.1029/2006JA012131.

Treumann, R. A. (2006), The electron cyclotron maser for astrophysical application, *Astron. Astrophys. Rev.*, *13*, 229–315, doi:10.1007/s00159-006-0001-y.

Winglee, R. M. (1985), Effects of a finite plasma temperature on electron-cyclotron maser emission, *Astrophys. J.*, *291*, 160–169, doi:10.1086/163052.

Wong, H. K., C. S. Wu, F. J. Ke, R. S. Schneider, and L. F. Ziebell (1982), Electromagnetic cyclotron-loss-cone instability associated with weakly relativistic electrons, *J. Plasma Phys.*, *28*, 503–525, doi:10.1017/S0022377800000453.

Wu, C. S., and L. C. Lee (1979), A theory of the terrestrial kilometric radiation, *Astrophys. J.*, *230*, 621–626, doi:10.1086/157120.

Wu, C. S., H. K. Wong, D. J. Gorney, and L. C. Lee (1982), Generation of the Auroral Kilometric Radiation, *J. Geophys. Res.*, *87*, 4476–4487, doi:10.1029/JA087iA06p04476.

Young, D. T., et al. (2004), Cassini plasma spectrometer investigation, *Space Sci. Rev.*, *114*, 1–112, doi:10.1007/s11214-004-1406-4.

Zarka, P. (2002), Radio and plasma waves at the outer planets, paper presented at the 34th COSPAR Scientific Assembly, Comm. on Space Res., Houston, Tex., 10–19 Oct.

Zarka, P., B. Cecconi, and W. S. Kurth (2004), Jupiter's low-frequency radio spectrum from Cassini/Radio and Plasma Wave Science (RPWS) absolute flux density measurements, *J. Geophys. Res.*, *109*, A09S15, doi:10.1029/2003JA010260.

C. Arridge and L. Lamy, Space and Atmospheric Physics, Imperial College London, London SW7 2AZ, UK. (csa@mssl.ucl.ac.uk; laurent.lamy@obspm.fr)

B. Cecconi, Observatoire de Paris, 5 place J. Janssen, F-92190 Meudon CEDEX, France. (baptiste.cecconi@obspm.fr)

D. A. Gurnett, W. Kurth, C. Lynch, J. D. Menietti, R. L. Mutel, and P. Schippers, Department of Physics and Astronomy, University of Iowa, Iowa City, IA 52242, USA. (donald-hurnett@uiowa.edu; william-kurth@uiowa.edu; christene-lynch@uiowa.edu; john-menietti@uiowa.edu; robert-mutel@uiowa.edu; patricia-schippers@uiowa.edu)